JOURNAL OF INTERNATIONAL CRISIS AND RISK COMMUNICATION RESEARCH
ISSN: 2576-0017
2024, VOL 7, NO S10

Evaluation of Numerical Techniques for Accurate Solution of the Eikonal Equation in a 3D Subsurface Medium: A Basis for Training Machine Learning Models

Francisco Gamboa Ortega[1], Luís Alfonso Guerra Hernández[2], Richard Eliseo Mendoza Gáfaro[3]

[1]Departamento de Física, Grupo Pangea, Universidad de Pamplona, Pamplona, Colombia.
[2]Grupo de Investigación Óptica Moderna-GOM, Departamento de Física, Facultad de Ciencias Básicas, Universidad de Pamplona, Pamplona, Colombia.
[3]Facultad de Ingenierías y Arquitectura, Grupo de Investigación de Inteligencia de Datos y Computación -GIIDAC.
[*]Corresponding author, e-mail: francisco.gamboa@unipamplona.edu.co

Abstract

This work presents the numerical techniques FMM (Fast Marching Method) and FSM (Fast Sweeping Method), along with their high-accuracy versions: HAFMM (High Accuracy Fast Marching Method) and HAFSM (High Accuracy Fast Sweeping Method), for solving the Eikonal equation. The accuracy of the classical and high-accuracy methods is compared using a proposed quantitative metric. The performance of the methods is evaluated on two three-dimensional models: one homogeneous and another heterogeneous with sharp interfaces, allowing for an analysis of the robustness and accuracy of each approach in contexts of varying complexity. Finally, the generalization capability of machine learning models is assessed by approximating the solution of the Eikonal equation using the most accurate method found in a three-dimensional heterogeneous subsurface medium when trained on artificially perturbed data.

Key words: HAFMM and HAFSM; Machine learning; Sharp interfaces.

1. Introduction

The Fast Marching Method (FMM) is a numerical algorithm that solves the Eikonal equation on a rectangular orthogonal grid. Since its introduction in 1995, the FMM has been applied in numerous fields, including robotics (Spira & Kimel, 2004), medical computer vision (Sethian, 1996), and geophysics, particularly to model the propagation of the first arrival of seismic waves (Luo et al., 2012; Qian and Symes, 2002; Zhang et al., 2021), as well as in Kirchhoff migration and travel-time tomography (Taillandier et al., 2009). Since then, several alternatives to the original method have been proposed with two main objectives: reducing computational time and improving accuracy. Another approach to solving the Eikonal equation is the Fast Sweeping Method (FSM), which, although already known in control theory, was first introduced in this context by Zhao (2004).

1.1 Eikonal Equation

The Eikonal equation can be directly derived from the acoustic wave equation with constant density in the frequency domain:

$$\nabla^2 U(x,\omega) + \omega^2 s^2 U(x,\omega) = 0, \qquad (1)$$

where $s(x)$ represents the slowness field, $U(\boldsymbol{x},\omega)$ is the pressure field at position $x=(x,y,z)$, and ω is the angular frequency. Assuming an impulsive source of the form $U(x,t)=A(x)\delta[t-\tau(x)]$ in a non-dispersive medium, its expression in the frequency domain is given by:

$$U(x,\omega)=A(x)e^{i\omega\tau(x)}, \tag{2}$$

where the constant-time surface $t=\tau(\mathbf{x})$ represents the wavefront. By substituting Equation 2 into Equation 1, we obtain:

$$[\omega^2 A(s^2-\nabla\tau\cdot\nabla\tau)+i\omega(A\nabla^2\tau+2\nabla A\cdot\nabla\tau)+\nabla^2 A]e^{i\omega\tau}=0. \tag{3}$$

For this expression to be valid for all ω, each coefficient must vanish independently, resulting in three differential equations:

$$\nabla^2 A=0, \tag{4}$$
$$A\nabla^2\tau+2\nabla A\cdot\nabla\tau=0, \tag{5}$$
$$s^2-\nabla\tau\cdot\nabla\tau=0. \tag{6}$$

Equation (4) models the attenuation of amplitude as it approaches the edges. Equation (5) is known as the transport equation and describes the evolution of the amplitude. Finally, Equation (6) is the Eikonal Equation, which represents the kinematics of the wavefront.

1.2 3D FMM and HAFMM algorithms

The FMM is a technique for modeling the evolution of closed surfaces such as wavefronts to determine the arrival time of the wavefront (Gómez et al., 2019). The method relies on a data structure to store and sequence the node updates (a heap structure) and on an *upwind* finite difference scheme to guarantee causality in the wavefront evolution. The upwind scheme for eikonal equation 6 is:

$$\begin{aligned}(\nabla\tau)^2\approx\Big[&\max\{D_{ijk}^{-x}\tau-D_{ijk}^{+x}\tau,0\}^2+\max\{D_{ijk}^{-y}\tau-D_{ijk}^{+y}\tau,0\}^2\\&+\max\{D_{ijk}^{-z}\tau-D_{ijk}^{+z}\tau,0\}^2\Big]=s^2,\end{aligned} \tag{7}$$

where:

$$\begin{aligned}D_{ijk}^{\pm x}\tau&=p_x\left(\tau_{i,j,k}-\tau_{i\pm1,j,k}\right),\\D_{ijk}^{\pm y}\tau&=p_y\left(\tau_{i,j,k}-\tau_{i,j\pm1,k}\right),\\D_{ijk}^{\pm z}\tau&=p_z\left(\tau_{i,j,k}-\tau_{i,j,k\pm1}\right),\end{aligned} \tag{8}$$

These are forward (+) or backward (−) finite difference schemes, where $p_x=\mp1/\Delta_x$, $p_y=\mp1/\Delta_y$ and $p_z=\mp1/\Delta_z$ store the finite difference coefficients and the grid spacings Δx, Δy and Δz (see Figure 1). By substituting Equation (8) into Equation (7), the neighboring point with the smallest value in the grid is selected to provide the maximum derivative, and the vertical and horizontal neighboring points are defined as:

$$\begin{aligned}\tau_x&=\min\left(\tau_{i+1,j,k},\,\tau_{i-1,j,k}\right),\\\tau_y&=\min\left(\tau_{i,j+1,k},\,\tau_{i,j-1,k}\right),\\\tau_z&=\min\left(\tau_{i,j,k+1},\,\tau_{i,j,k-1}\right).\end{aligned} \tag{9}$$

Rewriting Equation 7 in the form:

$$\max[p_x(\tau-\tau_x,0)]^2+\max\left[p_y\left(\tau-\tau_y,0\right)\right]^2+\max[p_z(\tau-\tau_z,0)]^2=s^2, \tag{10}$$

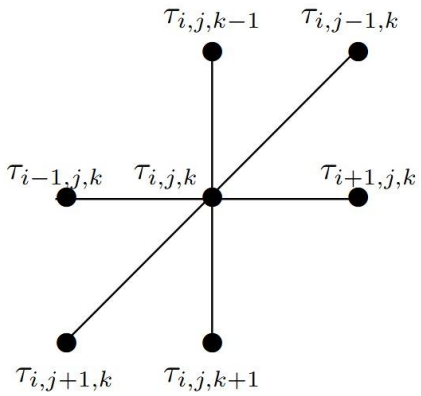

Figure 1. 3D update of the grid point.

Since the slowness is always positive ($(s > 0)$), τ must be greater than τ_z and τ_x, so it is safe to simplify Equation 10 to:

$$[p_x(\tau - \tau_x)]^2 + \left[p_y(\tau - \tau_y)\right]^2 + [p_z(\tau - \tau_z)]^2 = s^2. \quad (11)$$

Equation 11 is a quadratic polynomial of the form $a\tau^2 + b\tau + c = 0$ with coefficients:

$$\begin{aligned} a &= p_x^2 + p_y^2 + p_z^2 \\ b &= -2\left(p_x^2\tau_x + p_y^2\tau_y + p_z^2\tau_z\right) \\ c &= p_x^2\tau_x^2 + p_y^2\tau_y^2 + p_z^2\tau_z^2 - s^2. \end{aligned} \quad (12)$$

Whose result for Equation 7 is:

$$\tau^{xyz} = \frac{-b + \sqrt{b^2 - 4ac}}{2a}. \quad (13)$$

This is known as the three-sided update scheme. This quadratic form is only valid if $\tau^{xyz} \geq min(\tau_x, \tau_y, \tau_z)$. Some of the neighboring points may have infinite values (where the wavefront has not yet arrived). In this case, the causality condition $(b^2 > 4ac)$ fails, and it is necessary to use the one-sided update scheme by solving Equation 11 independently for each direction:

$$\tau^h = \tau_x + \frac{s}{|p_x|} \quad (14)$$

$$\tau^l = \tau_y + \frac{s}{|p_y|} \quad (15)$$

$$\tau^v = \tau_z + \frac{s}{|p_z|} \quad (16)$$

The final solution is the minimum between the three planes and the three-dimensional scheme:

$$\tau = \min(\tau^{xyz}, \tau^x, \tau^y, \tau^z). \quad (17)$$

The high-accuracy version of the FMM (HAFMM) differs only in the way the values of τ_x, τ_y, τ_z y τ_x, τ_y, p_x, p_y, p_z are chosen, to select between first- or second-order schemes in the finite difference operators. The second-order approximation of the finite difference operator is represented by:

$$D_2^{\pm x}\tau = p_x(\tau_{i,j,k} - \tau_x), \quad (18)$$

$$D_2^{\pm y}\tau = p_y(\tau_{i,j,k} - \tau_y), \quad (19)$$

$$D_2^{\pm z}\tau = p_z(\tau_{i,j,k} - \tau_z), \quad (20)$$

where:

$$\tau_x = \frac{1}{3}\left(4\tau_{i\pm1,j,k} - \tau_{i\pm2,j,k}\right), \tag{21}$$

$$\tau_y = \frac{1}{3}\left(4\tau_{i,j\pm1,k} - \tau_{i,j\pm2,k}\right) \tag{22}$$

$$\tau_z = \frac{1}{3}\left(4\tau_{i,j,k\pm1} - \tau_{i,j,k\pm2}\right), \tag{23}$$

$$p_x = \mp\frac{3}{2\Delta x}, \tag{24}$$

$$p_y = \mp\frac{3}{2\Delta y}, \tag{25}$$

$$p_z = \mp\frac{3}{2\Delta z}. \tag{26}$$

The criteria for choosing between forward or backward differences are initially the same as in the first-order scheme (Equation 9). Once the decision is made, it is necessary to verify whether finite values exist at the following two grid points to satisfy the causality condition $\tau_{i\pm1} > \tau_{i\pm2}$, allowing the use of the second-order scheme. If this condition is not met, the update continues using the first-order scheme.

1.3 3D FSM and HAFSM Algorithms

In the Fast Sweeping Method (FSM) algorithm, the *upwind* difference scheme used in the discretization enforces causality, meaning that the solution at a grid point is obtained solely from its neighboring values that are smaller (Jeong & Whitaker, 2008). The one-directional difference scheme ensures that information propagates from the interior outward, given that the data set Γ is contained within the computational domain. If all grid points can be ordered according to causality, a single Gauss-Seidel iteration is sufficient for convergence (Zhao, 2004). The key aspect of the method is to use Gauss-Seidel iterations with a different sweeping order in each iteration, maintaining causality according to the directions. The value at each grid point is always non-increasing during the iterations due to the update rule. Each time a grid point reaches the minimum possible value, that value is correct and will not be modified in subsequent iterations. The function used for a set Γ that satisfies the Eikonal Equation 1 is:

$$|\Delta d(x)| = 1, \quad d(x) = 0, \quad x \in \Gamma, \tag{27}$$

Where $d(x)$ denotes the distance function. All characteristics of this equation are straight lines emanating from the set Γ. In three dimensions, the upwind differentiation at the interior grid point i, j, k is given by:

$$\begin{aligned} & \left[p_x\left(\tau^{(x)}_{i,j,k} - min\left(\tau^{(x)}_{i-1,j,k}, \tau^{(x)}_{i+1,j,k}\right)\right)\right]^2 \\ + \quad & \left[p_y\left(\tau^{(y)}_{i,j,k} - min\left(\tau^{(y)}_{i,j-1,k}, \tau^{(y)}_{i,j+1,k}\right)\right)\right]^2 \\ + \quad & \left[p_z\left(\tau^{(z)}_{i,j,k} - min\left(\tau^{(z)}_{i,j,k-1}, \tau^{(z)}_{i,j,k+1}\right)\right)\right]^2 = s^2 \end{aligned} \tag{28}$$

Where $\tau^{(x)}_{i,j,k}$ is the numerical solution at $x_{i,j,k}$, $p_x = 1/\Delta_x$, $p_y = 1/\Delta_y$, $p_z = 1/\Delta_z$. The update of the distance value at the grid point i, j, k becomes:

$$\begin{aligned} \tau^{x_{\text{new}}}_{i,j,k} &= \min\left(\min\left(\tau^{(x)}_{i-1,j,k}, \tau^{(x)}_{i+1,j,k}\right) + \Delta_x, \tau^{(x)}_{i,j,k}\right), \\ \tau^{y_{\text{new}}}_{i,j,k} &= \min\left(\min\left(\tau^{(y)}_{i,j-1,k}, \tau^{(y)}_{i,j+1,k}\right) + \Delta_y, \tau^{(y)}_{i,j,k}\right), \\ \tau^{z_{\text{new}}}_{i,j,k} &= \min\left(\min\left(\tau^{(z)}_{i,j,k-1}, \tau^{(z)}_{i,j,k+1}\right) + \Delta_z, \tau^{(z)}_{i,j,k}\right). \end{aligned} \tag{29}$$

The distance value at any point on the grid can be computed from either its left or right neighbor exactly as:

$$\begin{aligned} d_x &= \min\left(d_{i-1,j,k}, d_{i+1,j,k}\right) + \Delta x, \\ d_y &= \min\left(d_{i,j-1,k}, d_{i,j+1,k}\right) + \Delta y, \\ d_z &= \min\left(d_{i,j,k-1}, d_{i,j,k+1}\right) + \Delta z. \end{aligned} \tag{30}$$

The first and second sweeps will cover the characteristics traveling from left to right, and vice versa; that is, the grid points whose values are determined by their left neighbors will be correctly computed in the first sweep. Similarly, in the second sweep, all grid points whose values depend on their right neighbors will also be correctly calculated. Since the current value is only updated if the newly computed value is smaller, the values that were correctly calculated in the first sweep will have already reached their minimum possible value and will not be modified during the second sweep. This same principle also applies when computing the perpendicular XZ plane. The high-accuracy version of FSM (HAFSM) differs only in how the values of τ_x, τ_y, τ_z and p_x, p_y, p_z are selected to apply either first- or second-order finite difference operators. The second-order formulation of the finite difference operator is, once again, represented by equations from 21 to 26. The criteria for deciding between forward or backward differencing are initially the same as in the first-order scheme (equations 9).

Once that decision is made, it is necessary to check whether finite values exist at the following two grid points to satisfy the causality condition, $\tau_{i\pm1} > \tau_{i\pm2}$ and thus continue with the second-order scheme.

If this condition is not met, the update proceeds using the first-order scheme. The HAFSM method is not used in the initial iterations since there are not enough available points for computation. However, error accumulation tends to decrease as the wavefront propagates.

2. Computational Experiments

To evaluate the accuracy, robustness, and efficiency of different approaches for estimating travel times in seismic media, a series of numerical experiments were carried out based on the implementation of the FMM and FSM methods, along with their high-accuracy versions, HAFMM and HAFSM. These techniques were applied to 2D and 3D seismic models, allowing for a comparative analysis across various scenarios.

The experiments include a comparison of the performance between classical and high-accuracy methods, an evaluation of their behavior in models with abrupt interfaces, the use of travel times generated by these physical methods to train and validate machine learning models, and the comparison of predictive performance when employing multiple training models. These analyses aim to identify the most efficient approach in terms of computational time and accuracy.

2.1 Analytical Solution vs. Algorithms in a 3D Homogeneous Medium

The first experiment presented in this work aims to evaluate the accuracy of the algorithms developed for solving the eikonal equation by comparing the travel times estimated by each method with a known analytical solution.

$$\tau(x, y, z) = \sqrt{(x - x_s)^2 + (y - y_s)^2 + (z - z_s)^2}, \tag{31}$$

where (x_s, y_s, z_s) corresponds to the source position. The calculation assumes that the source is located at the center of the model, $\tau(x_s, y_s, z_z) = 0$ the slowness is constant with a value of $s = 1\ m/s$, and the model dimensions are $50m^3$. The results, shown in Figures 2, demonstrate that the

HAFSM method exhibits a smaller error compared to the exact solution and other methods. This formulation allows for an objective, dimensionless comparison of the accuracy of each numerical technique. The evaluated methods include FMM, FSM, HAFMM, and HAFSM, where the latter two use second-order discretization. This experiment highlights the advantages of high-precision methods in reducing accumulated error and more accurately representing wavefront propagation, especially in regions with pronounced curvatures.

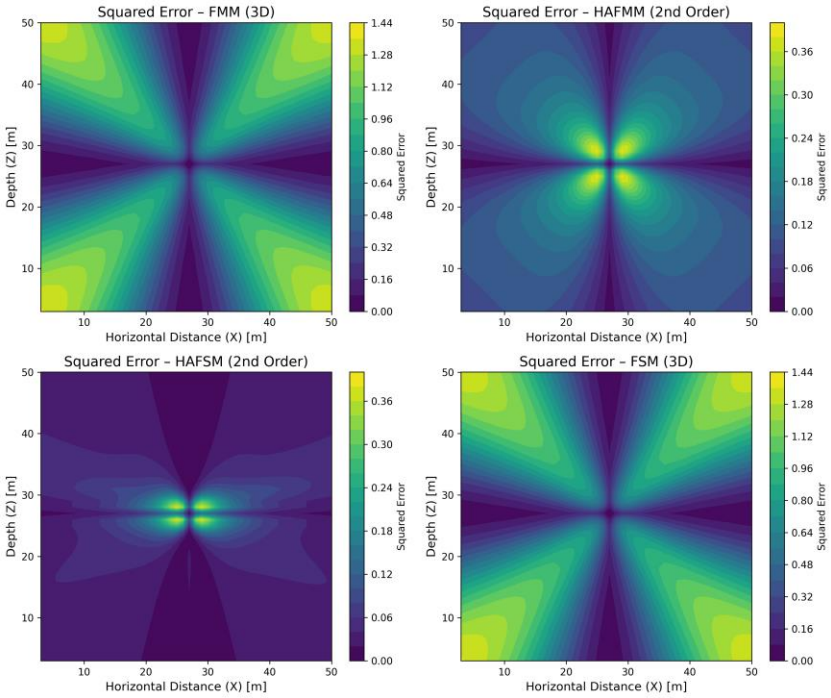

Figure 2. Mean squared error of the FMM, FSM methods and their respective high-precision versions HAFMM and HAFSM, using second-order discretization of derivatives, relative to the analytical function.

An increase in the order of derivative discretization in the developed schemes does not necessarily guarantee an improvement in modeling accuracy. This is evidenced in Figure 3, where the third-order discretization of the derivatives in equation 6 is compared for the HAFMM and HAFSM methods. Moreover, increasing the discretization order may result in a higher computational cost.

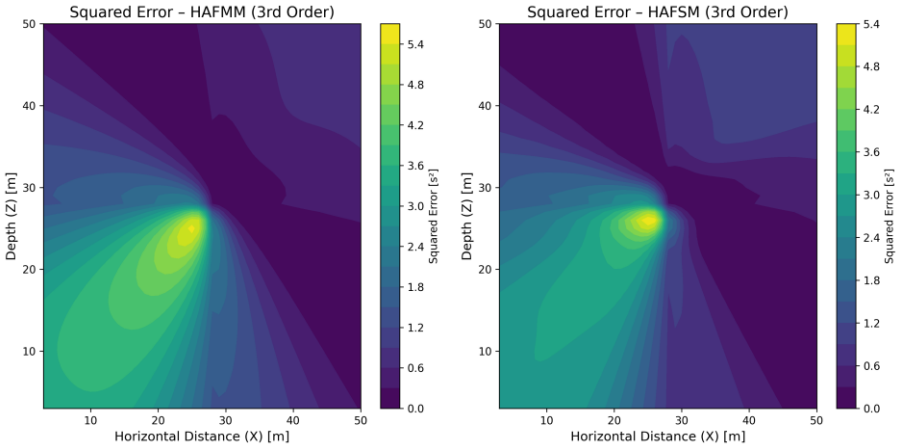

Figure 3. Mean squared error of the HAFMM and HAFSM methods, with the third-order discretization of derivatives, relative to the analytical function.

2.2 Global accuracy of the algorithms in a 3D heterogeneous medium

To evaluate the numerical accuracy of the FMM, FSM, HAFMM, and HAFSM methods beyond a visual inspection and across the entire model, a comparison was conducted based on how faithfully each method solves the eikonal equation 6, considering that:

$$|\nabla\tau(x,y,z)| = \frac{1}{v(x,y,z)} = s(x,y,z), \tag{32}$$

Where $\nabla\tau(x,y,z)$ represents the gradient of the travel time $\tau(x,y,z)$ computed by each method, $v(x,z)$ is the velocity of the medium, and $s(x,z)$ represents the slowness. The latter two fields are well-known and are used as a reference to locally evaluate differences and similarities between the medium's slowness and the value of $\nabla\tau(x,y,z)$. From this, the local error metric is defined as:

$$E(x,z) = |\,|\nabla\tau(x,y,z)| - s(x,z)\,|. \tag{33}$$

The evaluation focused on the regions of the model where significant velocity variations occur, that is, in the interface zones. In these areas, a Percentage Mean Squared Error (MSE%) was calculated, defined as:

The evaluation focused on regions of the model where significant velocity variations occur, that is, in the interface zones. In these areas, a Percent Mean Squared Error (MSE%) was calculated, defined as:

$$ECM\backslash\% = 100 \cdot \frac{\sum_{(x,y,z)\in\Omega} \left(|\nabla\tau(x,y,z)| - s(x,y,z)\right)^2}{\sum_{(x,y,z)\in\Omega}\left(\nabla\tau(x,y,z)\right)^2} \tag{34}$$

where Ω represents the interface zones, that is, where the velocities in the model change significantly.

The synthetic SEG/EAGE 3D *Overthrust* model was used as a test case to validate the three-dimensional discretization algorithms. This model represents an acoustic volume with constant density, defined on a uniform grid of $801 \times 801 \times 187$ samples. Geologically, it simulates a structure affected by erosion and compressional tectonics, with velocities ranging from 2178 to 6000 m/s. The results from all methods are presented in Figures 4, 5 y 6.

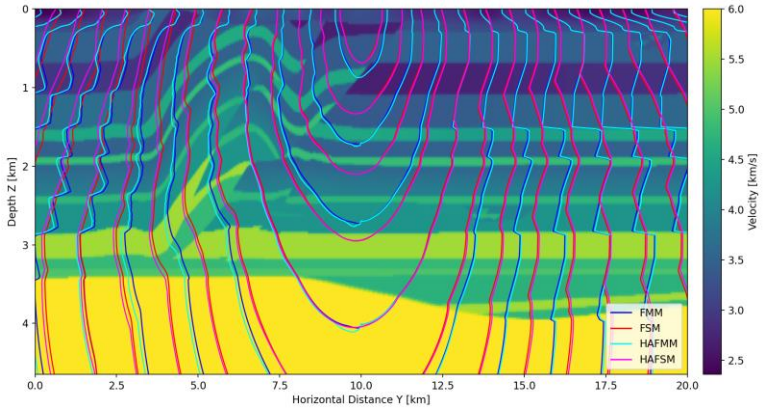

Metric	FMM	FSM	HAFMM	HAFSM	Best	Worst
ECM%	0.012343	0.000012	0.012643	0.000003	HAFSM	HAFMM

Figure 4. Inline cross-section of the velocity field and results from the algorithms: FMM (blue line), HAFMM (cyan line), FSM (red line), and HAFSM (magenta line), applied to the SEG/EAGE *Overthrust* model. The quantitative comparison between the time gradient $\tau(x,y,z)$ computed by each method and the velocity field is expressed through the MSE%. The source is located at $x = 10km$, $z = 2m$ on *inline* 400.

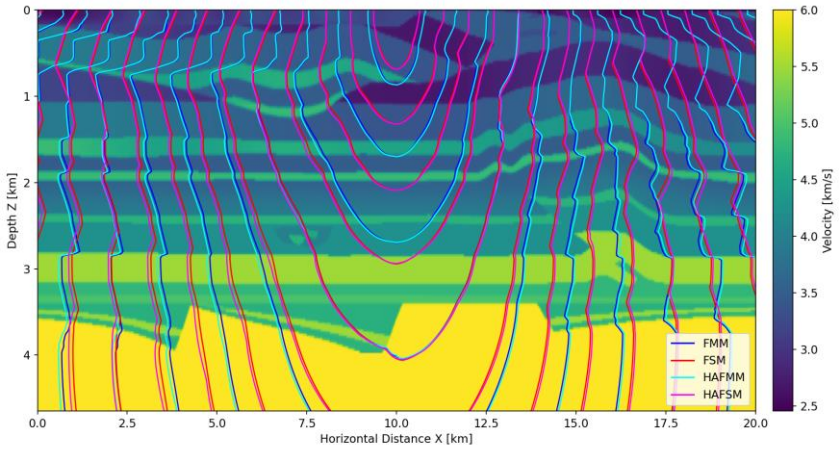

Metric	FMM	FSM	HAFMM	HAFSM	Best	Worst
ECM%	0.003576	0.000006	0.003579	0.000005	HAFSM	HAFMM

Figure 5. Xline cross-section of the velocity field and results from the algorithms: FMM (blue line), HAFMM (cyan line), FSM (red line), and HAFSM (magenta line), applied to the SEG/EAGE *Overthrust* model, along with the MSE%. The source is located at $x = 10km$, $z = 2m$, on *xline* 400.

In this context, it is observed that traditional methods, such as FMM and FSM, can exhibit significant differences compared to their high-accuracy counterparts, HAFMM and HAFSM, especially when the wavefront crosses regions with high velocities. The use of second-order discretizations in HAFMM and HAFSM helps reduce accumulated errors and mitigate errors associated with wavefront curvature.

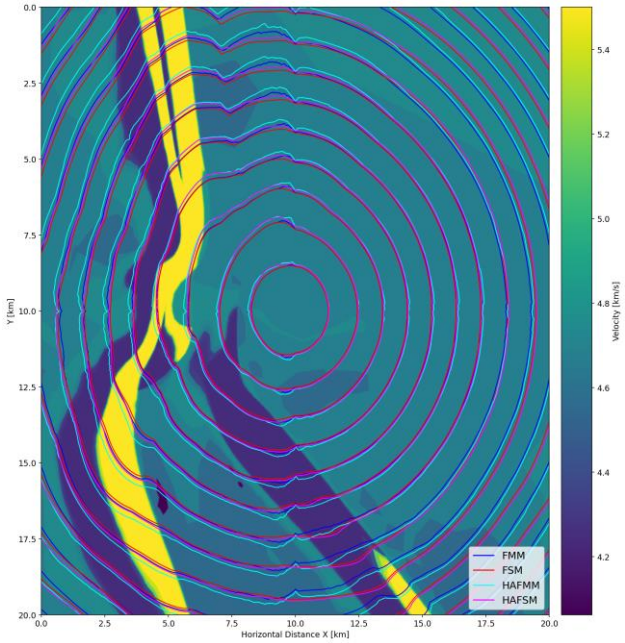

Metric	FMM	FSM	HAFMM	HAFSM	Best	Worst
ECM%	0.000014	0.000015	0.000016	0.000015	FMM	HAFMM

Figure 6. Plan view of the velocity field and results from the algorithms: FMM (blue line), HAFMM (cyan line), FSM (red line), and HAFSM (magenta line), applied to the SEG/EAGE *Overthrust* model, along with the MSE%. Source position: y = 10 km , x = 10 m on a slice with z = 2400m.

2.3 Local Accuracy of the Algorithms (XZ)

For this test, the section from Figure 5 is analyzed, and the results are presented in Figure 7. This figure shows the degree to which each method locally satisfies the eikonal equation by computing Equation 33, thereby illustrating the fidelity with which each method fulfills the eikonal equation.

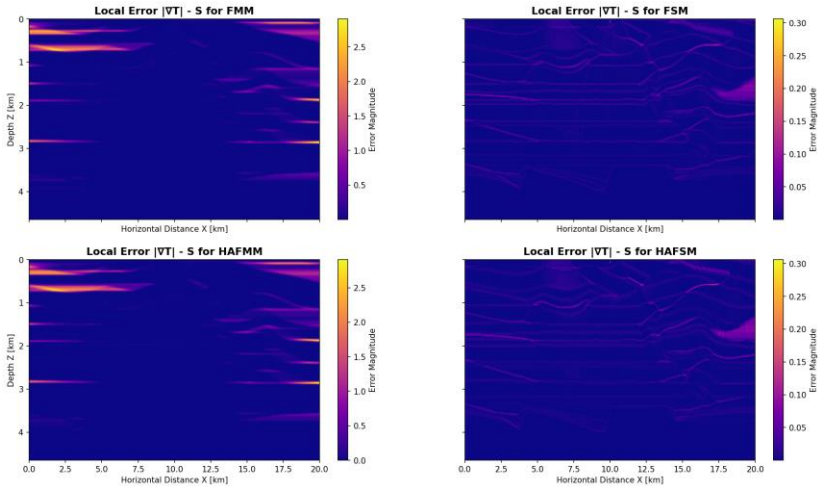

Figure 7. Local difference $E(x, z)$ computed using Equation 33, for all the methods studied, on the Xline section from Figure 5.

2.4 Local Accuracy of the Algorithms in the XY Plane

For this test, the section shown in Figure 6 is analyzed, and the results are presented in Figure 8. This figure shows the local error map in a plan view section centered around the source for the four methods analyzed. Unlike the cross-sectional view, in this case, the wavefront exhibits a more symmetrical radial propagation with oblique and curved trajectories.

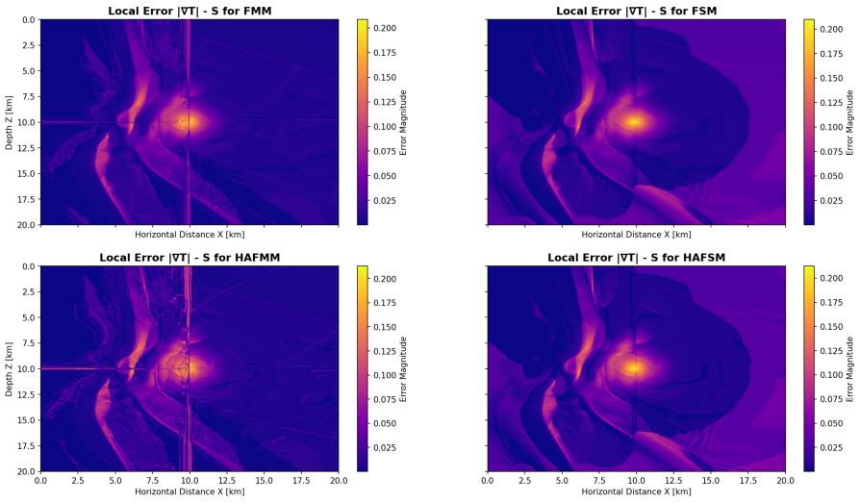

Figure 8. Local difference $E(x, z)$ calculated using equation 33, for all the methods studied, in the plan view section of Figure 6.

Figure 7 shows that the FMM and HAFMM methods (top left and bottom left, respectively) exhibit significant local errors in areas near the source and in horizontal interfaces or regions with abrupt contrasts. Although these methods are efficient in adaptively propagating the wavefront, interpolation in the regions with velocity changes can introduce localized errors of considerable magnitude, exceeding values of 2.5 in the case of FMM. On the other hand, the FSM and HAFSM methods (top and bottom right) exhibit a more uniform error distribution, with maximum values on the order of 0.3. These methods, based on fixed directional sweeps, preserve the local fulfillment of the eikonal equation in smooth regions. However, they exhibit systematic errors in oblique or curved structures, highlighting their sensitivity to the wavefront geometry and its alignment with the Cartesian grid.

The FMM and HAFMM methods (left) show a notable increase in the complexity of the error pattern compared to the XZ case. Linear and radial structures are evident, with localized errors at interface edges or in areas with high wavefront curvature. Although the maximum error values do not exceed 0.2, the spatial distribution is broader, with larger affected regions compared to the cross-sectional view. This is due to the method's difficulty in accurately interpolating travel times in arbitrary directions and the resulting increase in angular dispersion. On the other hand, the FSM and HAFSM methods (right) maintain a smoother error distribution. However, they also show an increase compared to the cross-sectional case, especially in areas where the wavefront propagation does not align with the preferred sweep directions. While the maximum error values remain similar (0.2), regions affected by moderate errors (0.05–0.1) are more extensive, particularly along the diagonals.

3. Approximate Solution of the Eikonal Equation Using Machine Learning

Traditionally, the Eikonal equation is solved using numerical methods Waheed, et al. (2020). In this work, we propose an alternative approach: training a machine learning model to approximate the solution of equation 1, using the spatial coordinates and velocity as input variables $x = (x, y, z, v)$, and the label computed using the HAFSM method, $y = \tau(x)$. The objective is to find a function $\hat{T}(x; \theta)$ such that:

$$\hat{T}(x; \theta) \approx \tau(x), \tag{35}$$

where θ represents the internal parameters of the model (weights in a neural network, splits in a *decision tree*, etc.). To quantify the quality of the approximation, the percentage mean squared error between the reference solution (HAFSM) and the trained solution $\hat{T}(x)$ is included.

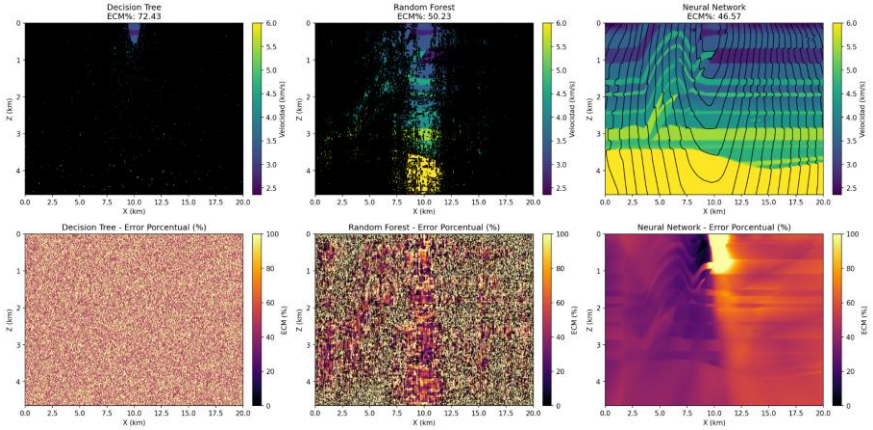

Figure 9. Comparison of the performance of three machine learning models in predicting arrival times $\tau(x, z)$ in a subsurface medium. The top row shows the velocity field $v(x, z)$ along with contour lines of the predicted times. The bottom row represents the percentage error (MSE%), calculated with respect to a reference solution obtained using the HAFSM method. The models were trained with time data systematically modified by ±200%.

In the experiment shown in Figure 9, three models were trained: a Decision Tree Regressor, a Random Forest Regressor, and a Neural Network. The objective of the experiment is to test whether machine learning models can learn the underlying spatial relationships between the coordinates (x, z), the local velocity ($v(x, z)$, and the arrival time $\tau(x, z)$, even when the training data are systematically altered (up to ±200%) relative to an accurate reference solution. Another result from Figure 9 is that the ML models manage to approximate the solution of the eikonal equation with good fidelity without the need to solve it explicitly (Yuan et al. (2020); Smith and Cockett (2021); Sun and Fomel (2015)). The use of HAFSM as the reference ground truth allows the model to learn from a highly accurate solution. This approach demonstrates that machine learning can serve as a fast and generalizable solver for the eikonal equation, making it ideal for applications in migration, inversion, and real-time simulation.

Conclusions

The HAFSM method exhibited the lowest root-mean-square error relative to the exact solution when compared to the other methods, both in homogeneous and heterogeneous velocity media. Increasing the spatial derivative discretization to third order did not improve the accuracy of the methods (see Figures 2 and 3). Although computation time was not measured, this increase in discretization order is expected to result in higher computational costs. The results for the horizontal (planar) section present a greater numerical challenge for all evaluated methods due to the need to adapt to trajectories that are not aligned with the computational grid. This increase in local error in the horizontal plane, relative to the vertical cross-section, is consistent with previously observed trends in the global error metric ECM% (see comparison tables), and reinforces the importance of considering the wavefront geometry when selecting a solution method.

In the simulations shown in Figures 4 and 5, the visual alignment between travel time contours and geological interfaces does not always match the ECM% values. This is because smoother methods—such as FSM and HAFSM—can produce visually less abrupt but numerically more consistent solutions in terms of gradient continuity. In contrast, methods such as FMM and HAFMM may delineate interfaces more sharply yet exhibit greater local errors in the numerical derivation of the travel time field.

In the horizontal section of Figure 6, the wavefront propagates from a fixed depth outward in the X-Y directions, imposing challenges on methods that update only in fixed directions (X-Z or Y-Z). The FSM method uses eight fixed sweeping directions (top-left, top-right, etc.). It, therefore, does not adapt well to smooth diagonal trajectories present in the horizontal section—where FMM performs better.

Overall, the results indicate that FSM and HAFSM offer better local error control. In contrast, FMM and HAFMM, although more versatile in complex geometries, require careful grid design and interpolation handling to avoid significant numerical errors. The choice of method thus depends on the trade-off between global accuracy and local fidelity, depending on the specific geophysical application.

References

Gómez, J., Garrido, D., Álvarez, S., & Moreno, L. (2019). Fast methods for eikonal equations: An experimental survey. *IEEE Access, 7*, 39005–39029. https://doi.org/10.1109/ACCESS.2019.2906782

Waheed, U. B., Haghighat, E., Alkhalifah, T., Song, C., & Hao, Q. (2020). *Eikonal solution using physics-informed neural networks*. In Proceedings of the EAGE 2020 Annual Conference &

Exhibition Online (pp. 1–5). European Association of Geoscientists & Engineers. https://doi.org/10.3997/2214-4609.202011041

Jeong, W.-K., & Whitaker, R. T. (2008). A fast iterative method for eikonal equations. *SIAM Journal on Scientific Computing, 30*(5), 2512–2534. https://doi.org/10.1137/060670298

Luo, S., Qian, J., & Zhao, H. (2012). Higher-order schemes for 3D first-arrival traveltimes and amplitudes. *Geophysics, 77*(2), T47–T56. https://doi.org/10.1190/geo2010-0363.1

Qian, J., & Symes, W. W. (2002). A fast marching method for computing traveltimes in inhomogeneous anisotropic media. *Geophysics, 67*(2), 516–523.

Sethian, J. A. (1996). Fast marching level set method for monotonically advancing fronts. *Proceedings of the National Academy of Sciences, 93*, 1591–1595. https://doi.org/10.1016/j.jcp.2016.08.012

Smith, A., & Cockett, R. (2021). Numerical methods for the eikonal equation in geophysical applications. Computers & Geosciences, 147, 104662.

Spira, A., & Kimel, R. (2004). An efficient solution to the eikonal equation on parametric manifolds. *Interfaces and Free Boundaries, 6*, 315–328. https://doi.org/10.4171/IFB/102

Sun, Y., & Fomel, S. (2015). Low-rank approximation of the eikonal solver for computing traveltime fields. Geophysics, 80(3), WA87–WA100.

Taillandier, C., Noble, M., Chauris, H., & Calandra, H. (2009). First-arrival traveltime tomography based on the adjoint-state method. *Geophysics, 74*(6), WCB1–WCB10. https://doi.org/10.1190/1.3250266

Yuan, S., Shah, A., Richardson, A., Ananthanarayanan, V., & Meade, B. J. (2020). EikoNet: Solving the eikonal equation with deep learning. *arXiv preprint*, arXiv:2004.00361. https://arxiv.org/abs/2004.00361

Zhang, Q., Ma, X., & Nie, Y. (2021). An iterative fast sweeping method for the eikonal equation in 2D anisotropic media on unstructured triangular meshes. *Geophysics, 86*(3), U49–U61. https://doi.org/10.1190/geo2020-0187.1

Zhao, H. (2004). A fast sweeping method for eikonal equations. *Geophysics, 74*, 603–627. https://doi.org/10.1090/S0025-5718-04-01678-3

Acknowledgments

Not applicable.

Ethics Approval and Consent to Participate

Not applicable.

Consent for Publication

Not applicable.

Availability of data and material

Data and materials will be available upon request to the authors.

Competing Interests

The authors declare no competing interests.

Funding

Not applicable.

Author contributions

Francisco Gamboa Ortega: Writing – original draft, Formal analysis, Data curation, Supervision, Methodology, Investigation. **Luis Alfonso Guerra-Hernández:** Writing – review & editing, Formal analysis, Data curation, Investigation. **Richard Eliseo Mendoza Gáfaro:** Writing – review & editing, Formal analysis, Data curation, Investigation.